

Compressed sensing for longitudinal MRI: An adaptive-weighted approach

L. Weizman^{a,*}, Y.C. Eldar^a, D. Ben Bashat^b

^a*Department of Electrical Engineering, Technion - Israel Institute of Technology, Israel*

^b*Tel Aviv Medical Center, Tel Aviv University, Israel*

Abstract

Purpose: Repeated brain MRI scans are performed in many clinical scenarios, such as follow up of patients with tumors and therapy response assessment. In this paper, the authors show an approach to utilize former scans of the patient for the acceleration of repeated MRI scans.

Methods: The proposed approach utilizes the possible similarity of the repeated scans in longitudinal MRI studies. Since similarity is not guaranteed, sampling and reconstruction are adjusted during acquisition to match the actual similarity between the scans. The baseline MR scan is utilized both in the sampling stage, via adaptive sampling, and in the reconstruction stage, with weighted reconstruction. In adaptive sampling, k -space sampling locations are optimized during acquisition. Weighted reconstruction uses the locations of the nonzero coefficients in the sparse domains as a prior in the recovery process. The approach was tested on 2D and 3D MRI scans of patients with brain tumors.

Results: The longitudinal adaptive CS MRI (LACS-MRI) scheme provides reconstruction quality which outperforms other CS-based approaches for rapid MRI. Examples are shown on patients with brain tumors and demonstrate improved spatial resolution. Compared with data sampled at Nyquist rate, LACS-MRI exhibits Signal-to-Error Ratio (SER) of 24.8dB with undersampling factor of 16.6 in 3D MRI.

Conclusions: The authors have presented a novel method for image

*Corresponding author

Email addresses: weizmanl@tx.technion.ac.il (L. Weizman),
yonina@ee.technion.ac.il (Y.C. Eldar), dafnab@tasmc.health.gov.il (D. Ben Bashat)

reconstruction utilizing similarity of scans in longitudinal MRI studies, where possible. The proposed approach can play a major part and significantly reduce scanning time in many applications that consist of disease follow-up and monitoring of longitudinal changes in brain MRI.

Keywords: Rapid MR, Compressed Sensing, Longitudinal studies

1. Introduction

Repeated brain MRI scans are performed in many clinical scenarios, such as follow up of patients with tumors and therapy response assessment (Rees et al., 2009; Young et al., 2011; Weizman et al., 2012; Yip et al., 2014; Weizman et al., 2014). They constitute one of the most efficient tools to track pathology changes and to evaluate treatment efficacy in brain diseases. In many cases most of the imaging data of the repeated scan is already present in the former scan. In this paper we aim at exploiting this temporal similarity in MRI longitudinal studies for rapid MRI acquisition of the repeated scan.

The use of a reference image in medical image reconstruction is quite established and is popular in various imaging modalities. Examples include computed tomography (Chen et al., 2008; Lauzier et al., 2012), spectroscopic imaging (Hu et al., 1988), imaging of contrast agent uptake (Van Vaals et al., 1993), dynamic MRI (Jones et al., 1993; Liang and Lauterbur, 1994; Korosec et al., 1996; Madore et al., 1999; Tsao et al., 2003; Mistretta et al., 2006) and real time tracking of tumors (Yip et al., 2014), locally-focused MRI (Cao et al., 1995) and feature-recognizing MRI (Cao and Levin, 1993).

Since the introduction of Compressed Sensing (CS) (Candès, 2006; Donoho, 2006; Eldar and Kutyniok, 2012) to the field of MRI (Lustig et al., 2007), the use of a reference image has been exploited within CS, such as in rapid dynamic MRI, by exploiting temporal sparsity. Gamper et al. perform randomly skipping phase-encoding lines in each dynamic frame to speed-up acquisition (Gamper et al., 2008). Liang et al. propose an iterative algorithm to detect the signal support in CS dynamic MRI (Liang et al., 2012). Zonooni and Kassim use the previous time-frame in dynamic MRI to weight the ℓ_1 minimization in the CS reconstruction process (Zonoobi and Kassim, 2013). Trzasko et al. exploit a pre-injection background image (Trzasko et al., 2011) and Wu et al. utilize a constraining image to enhance MR angiography (MRA), while incorporating CS and parallel imaging (Wu et al., 2008).

Samsonov et al. (Samsonov et al., 2010) have suggested using a reference frame to speed-up MRI in longitudinal studies. Their approach, as well as most other approaches that exploit a reference image in MRI applications, rely on similarity between the reference scan and the current scan. The similarity assumption is indeed valid in cases where imaging data consists of many images acquired at a high frame rate.

However, longitudinal MRI poses a different challenge due to the large time gaps between the scans. On the one hand, similarity across time points is not guaranteed, since in many cases we observe vast changes between scans due to pathology changes or surgical interventions. In addition, undersampling in the time domain is impractical, due to the demand for high quality reconstruction at each time point. Therefore, reconstruction errors in this single time-frame imaging modality cannot be compensated for by adjacent time-frames like in dynamic imaging. On the other hand, in cases where similarity between previous and current scans does exist, the high resolution former scan of the patient may constitute a very strong prior for the reconstruction of the repeated scan. Therefore, for the scenario of longitudinal MRI, we suggest exploiting the former scan in an adaptive manner. The similarity of the reference scan to the current scans is “learned” during the acquisition process, leading to an iterative update of sampling and reconstruction accordingly.

In the context of MRI, image reconstruction quality highly depends on the \mathbf{k} -space sampling pattern (Tsai and Nishimura, 2000; Knoll et al., 2011). The concept of adaptive sampling (a.k.a “adaptive sensing”) suggests that samples are selected sequentially, where the choice of the next samples may depend on previously gathered information. This concept has been implemented previously, mainly for dynamic MRI (Panych and Jolesz, 1994; Yoo et al., 1999), and was later extended and implemented in a CS framework (Seeger et al., 2010; Ravishankar and Bresler, 2011a,b). In this work we utilize this concept and explore whether we can adaptively optimize the sampling pattern on-the-fly, based on partial reconstruction results from previously acquired samples in longitudinal MRI.

A substantial body of mathematical theory has recently been published establishing the basic principles of adaptive sampling of sparse signals (Haupt et al., 2011; Wei and Hero, 2013; Chen et al., 2014). According to these mathematical results, reconstruction from samples selected sequentially, based on partial reconstruction results is significantly improved versus reconstruction from non-adaptive (deterministic or random) samples.

Knowledge of the former scan can be advantageously used not only to design an adaptive sampling pattern, but also to improve image reconstruction from sampled data. This improvement can be obtained via the definition of regularization weights in the reconstruction optimization problem (Candes et al., 2008; Haldar et al., 2008; Vaswani and Lu, 2010). We apply this approach, coined “weighted reconstruction”, for the scenario of longitudinal MRI. This weighting mechanism allows to relax or enforce the demand for sparsity according to the level of similarity between the current scan and the reference scan.

In this paper we develop a framework for CS longitudinal MRI, by employing the two well established approaches above in parallel: adaptive sampling and weighted reconstruction. In this way, we exploit the prior scan of the patient to reconstruct the repeated scan from highly undersampled \mathbf{k} -space data. To keep the discussion as simple as possible, we focus on Cartesian sampling for brain MRI.

The novelty of this paper lies in the unique implementation of weighted reconstruction and adaptive sampling for the scenario of longitudinal studies, where the temporal similarity is not taken for granted. Unlike traditional CS MRI approaches that utilize prior constraints, in our approach the temporal similarity assumption is continuously examined, and the sampling and reconstruction algorithms are updated accordingly. Experimental results exhibit the superiority of the proposed method regardless of the validity of the temporal similarity assumption in the examined cases.

This paper is organized as follows. Section 2 presents the theory of weighted reconstruction and adaptive sampling and their implementation for longitudinal MRI. Section 3 describes the experimental results. Section 4 discusses practical issues related to the implementation of the method in real time applications; Section 5 concludes by highlighting the key findings of the research.

2. Method

2.1. Summary of Compressed Sensing MRI

The application of CS for rapid MRI (Lustig et al., 2007) exploits the fact that MRI scans are typically sparse in some transform domain, which is incoherent with the sampling domain. Nonlinear reconstruction is then used to enforce both sparsity of the image representation and consistency with the

acquired data. A typical formulation of CS MRI recovery aims to solve the following constrained optimization problem:

$$\min_{\mathbf{x}} \quad \|\Psi \mathbf{x}\|_1 \quad \text{s.t.} \quad \|\mathbf{F}_u \mathbf{x} - \mathbf{y}\|_2 < \epsilon \quad (1)$$

where $\mathbf{x} \in \mathbb{C}^N$ is the N -pixel complex image to be reconstructed, represented as a vector, $\mathbf{y} \in \mathbb{C}^M$ represents the \mathbf{k} -space measurements, \mathbf{F}_u is the under-sampled Fourier transform operator, Ψ is a sparsifying transform operator and ϵ controls the fidelity of the reconstruction to the measured data.

This fundamental CS MRI formulation is the basis for many MRI reconstruction applications, where the sparse transform domain varies depending on the particular setting. In MR angiography, where images are truly sparse, finite-differences is used as a sparsifying transform. In dynamic MRI, the difference between adjacent time frames is sparse (Lang and Ji, 2008; Jung et al., 2009; Gamper et al., 2008). Sparsity can also be exploited in multiple domains, for example in both temporal and spatial domains (Lustig et al., 2006).

Here, we focus on Cartesian sampling, so that \mathbf{F}_u represents lines samples of the \mathbf{k} -space in 2D imaging. We further consider brain MRI, known to be sparse in the wavelet domain. Therefore, we will assume throughout that Ψ is an appropriately chosen wavelet transform.

2.2. The sparsity of longitudinal MRI scans

In longitudinal studies, patients are scanned every several weeks or months. This scanning scheme is broadly used, for follow-up purposes and for therapy response assessment. In this setting, we could save scanning time if we are able to scan only the changes from the baseline. This type of scanning is, of course, not feasible, due to practical difficulties in designing such a sequence and the fact that prior information on the changes is mostly unavailable.

While the scenario of longitudinal studies is fundamentally different from dynamic MRI in many aspects, we still find that similarity across time points exists in many cases. Figure 1 shows an example of the same axial slice taken from multiple scans acquired from a patient with Optic Pathway Glioma (OPG), demonstrating a relatively slow growing tumor pattern. The bottom row of the figure shows the representation of each time point in Daubechies-4 wavelet transform (Daubechies et al., 1992), which is widely used as a sparse transform for brain MRI. The similarity between image slices acquired at several time points is clearly demonstrated. Moreover, the representation of

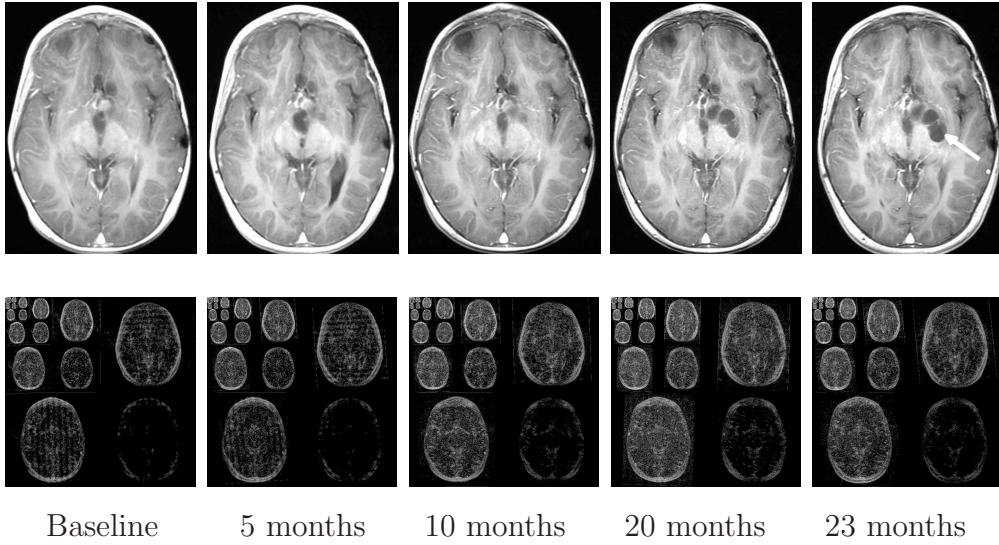


Figure 1: Brain contrast-enhanced T1-weighted longitudinal scans of patient with Optic Pathway Gliomas (OPG). The same spatial slice (top) and its representation in the wavelet domain (bottom) are shown before treatment (leftmost image) and 5, 10, 20 and 23 months after the beginning of treatment. It can be seen that despite the cyst evolving over time (marked by an arrow in the rightmost image) many image regions remain unchanged from one time point to another. Moreover, the support of the image in the wavelet domain (bottom) is preserved with no major changes over time (the minor structured artifacts in the wavelet domain are related to image registration between time points).

the images in the wavelet domain is sparse, and the locations of the dominant wavelet coefficients (a.k.a the support of the image in the wavelet domain) are similar across the patient’s time points.

Exploiting temporal similarity can be embedded in (1) by an additional term, which will promote sparsity of the difference between the image to be reconstructed, \mathbf{x} , and a previously acquired image of the same patient, \mathbf{x}_0 . This leads to the modified problem:

$$\min_{\mathbf{x}} \underbrace{\|\Psi\mathbf{x}\|_1}_{\text{term 1}} + \lambda \underbrace{\|\mathbf{x} - \mathbf{x}_0\|_1}_{\text{term 2}} \quad \text{s.t.} \quad \|\mathbf{F}_u\mathbf{x} - \mathbf{y}\|_2 < \epsilon. \quad (2)$$

Here, *term 1* enforces sparsity of \mathbf{x} in the wavelet domain, and *term 2* enforces similarity of \mathbf{x} to \mathbf{x}_0 in the image domain. The parameter λ trades sparsity in the wavelet domain with sparsity in the temporal domain. This approach of utilizing sparsity in both spatial and temporal domains via CS is coined hereinafter TCS-MRI (Temporal Compressed Sensing).

Note that *term 2* is sparse if there are no major changes between \mathbf{x} and \mathbf{x}_0 , both images have similar grey-level intensities and they are spatially matched. While these conditions meet in many application of dynamic imaging, such as prior image constrained compressed sensing (PICCS) in CT (Chen et al., 2008; Lauzier et al., 2012) and dynamic MRI (Jung et al., 2009; Lustig et al., 2006; Gamper et al., 2008; Yip et al., 2014), in longitudinal MRI none of these requirements are guaranteed. While there are solutions for miss-registration and variable grey level intensities (see Section 4), the temporal similarity in longitudinal MRI is a-priori unknown. Although longitudinal MRI may exhibit temporal similarity (Samsonov et al., 2010), we have to take into account that in many cases the follow-up scan may exhibit substantial changes with respect to the baseline scan. Such cases may occur, for example, if a surgical intervention was applied between the time points or if there is a major progressive or therapy response. Figure 2 shows two representative examples.

Therefore, using (2) for image reconstruction under the assumption of substantial similarity between time points might result in improper reconstruction in cases where this assumption does not hold. To avoid this we have to carefully design a sampling and reconstruction mechanism that will be adjusted to match the temporal similarity of the case at hand. To achieve this goal, we extend TCS-MRI using weighted reconstruction and adaptive sampling.

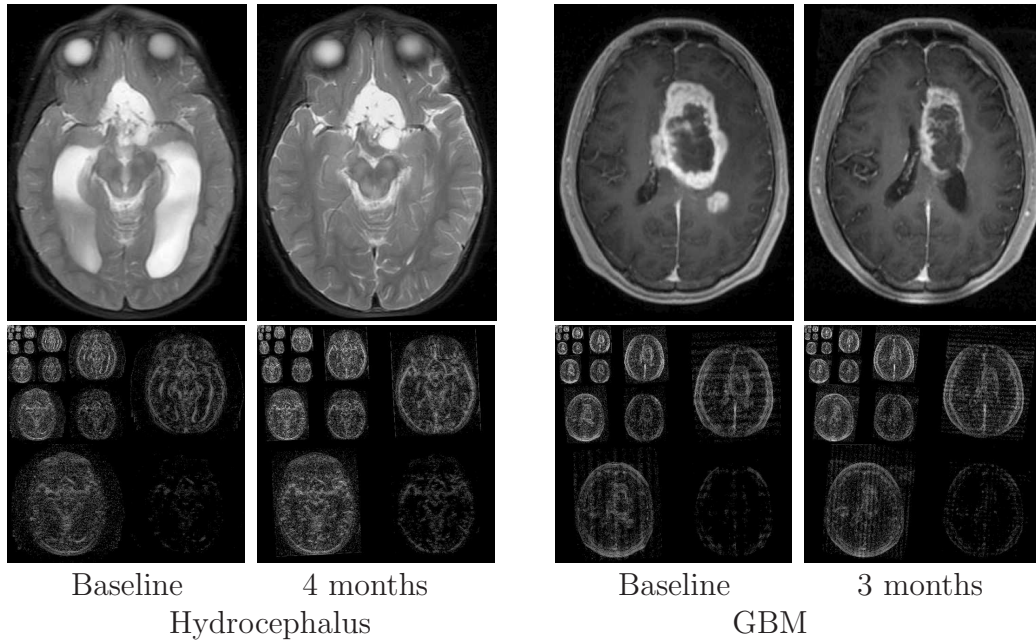


Figure 2: Left: Brain T2-weighted consecutive scans of a patient with Hydrocephalus. Scans were acquired before and after treatment. Right: contrast-enhanced T1-weighted consecutive scans of a patient with Glioblastoma multiforme (GBM) acquired during the treatment period. In these cases, there is substantial difference over time between the consecutive scans of the patients, in both the image (top) and the wavelet (bottom) domains.

2.3. Adaptive sampling and Weighted reconstruction

Many extensions have been proposed to improve the performance of the sampling and reconstruction phases. One of these extensions consists of embedding prior knowledge for better recovery by weighted reconstruction, which has been examined in many image reconstruction problems (Fessler et al., 1992; Hero et al., 1999; Haldar et al., 2008) and also in the context of CS (Vaswani and Lu, 2010; Khajehnejad et al., 2009; Friedlander et al., 2012). Weighted reconstruction can be mathematically embedded into the basic CS equation (1) by adding a diagonal weighting matrix, $\mathbf{W} = \text{diag}([w_1, w_2, \dots, w_N])$, to embed prior knowledge on the support, as proposed by Candes et al. (Candes et al., 2008):

$$\min_{\mathbf{x}} \quad \|\mathbf{W}\Psi\mathbf{x}\|_1 \quad \text{s.t.} \quad \|\mathbf{F}_u\mathbf{x} - \mathbf{y}\|_2 < \epsilon \quad (3)$$

where w_i represents the probability that $i \notin T$, and T is the support of \mathbf{x} in the sparse transform domain. It has been shown that weighted reconstruction outperforms traditional CS-MRI for dynamic MRI (Vaswani and Lu, 2010; Zonoobi and Kassim, 2012), where the support of the previous time frame is used as an estimate for the support of the current frame.

Prior knowledge can also be used to optimize the way that data is acquired (Zientara et al., 1994; Nagle and Levin, 1999; Gao and Reeves, 2000). However, since in longitudinal MRI the similarity between scans is not guaranteed, an adaptive mechanism is needed to determine the level of similarity between scans. Adaptive sampling proposes a selective sample selection, where the choice of the next samples depends on the previously gathered information. It has been proposed to improve signal's support detection from low number of samples or under a constraint on the total sensing effort (Haupt et al., 2009, 2011; Wei and Hero, 2013). The rationale behind this approach is that the estimation error one can get by using clever sampling based on previously acquired data, is generally lower than that achievable by a non-adaptive scheme. While Arias-Castro et al. (Arias-Castro et al., 2013) have shown that the validity of this claim is limited in general, it is proven to be valid for many cases.

In MRI, Seeger et al. (Seeger et al., 2010) employ this concept to optimize \mathbf{k} -space trajectories, by formulating the optimization problem as a Bayesian experimental design problem. They use the posterior uncertainty as the criterion for selecting the next trajectory at each round. Ravishankar and Bresler (Ravishankar and Bresler, 2011a) propose an adaptive scheme

that relies on training image scans to optimize the sampling pattern. Their criterion takes into account training data and the reconstruction strategy.

In the application of CS for longitudinal studies we use weighted reconstruction and adaptive sampling in a “patient-specific” way: \mathbf{k} -space trajectories will be optimized based on the past scan of the patient currently being scanned and reconstruction is improved via weighted reconstruction. In addition, this approach will iteratively detect cases in which the assumption of temporal similarity does not hold, and will update the sampling and reconstruction processes accordingly.

2.4. Adaptive-Weighted CS for Longitudinal MRI

Embedding weighted reconstruction into the longitudinal MRI results in the following minimization problem:

$$\min_{\mathbf{x}} \underbrace{\|\mathbf{W}_1 \Psi \mathbf{x}\|_1}_{\text{term 1}} + \lambda \underbrace{\|\mathbf{W}_2 (\mathbf{x} - \mathbf{x}_0)\|_1}_{\text{term 2}} \quad \text{s.t.} \quad \|\mathbf{F}_u \mathbf{x} - \mathbf{y}\|_2 < \epsilon \quad (4)$$

where \mathbf{W}_k is a diagonal matrix, $\mathbf{W}_k = \text{diag}([w_k^1, w_k^2, \dots, w_k^N])$ and w_k^i controls the weight given to each element in the support of *term 1* or *term 2*. Adding \mathbf{W}_1 to *term 1* relaxes the demand for sparsity on the elements in the support of the image in its sparse transform domain. As a result, sparsity in the wavelet domain is strongly enforced on elements outside of the support. Adding \mathbf{W}_2 to *term 2* controls the demand for similarity between \mathbf{x} and \mathbf{x}_0 . As a result, sparsity is enforced only in image regions where \mathbf{x} and \mathbf{x}_0 are similar.

The solution of problem (4) can be obtained via extending one of the well-known approaches for the classical CS problem (Donoho and Tsaig, 2008; Becker et al., 2011). In our experiments, we extended the fast iterative shrinkage-thresholding algorithm (FISTA) (Beck and Teboulle, 2009) to solve the unconstrained problem in so-called Lagrangian form:

$$\min_{\mathbf{x}} \|\mathbf{F}_u \mathbf{x} - \mathbf{y}\|_2^2 + \lambda_1 \underbrace{\|\mathbf{W}_1 \Psi \mathbf{x}\|_1}_{\text{term 1}} + \lambda_2 \underbrace{\|\mathbf{W}_2 (\mathbf{x} - \mathbf{x}_0)\|_1}_{\text{term 2}} \quad (5)$$

The values of λ_1 and λ_2 can be selected appropriately such that the solution of (5) is exactly as (4), for a given λ . These values control the trade-off between enforcing sparsity in the wavelet and temporal domains. Detailed implementation of our FISTA-based approach can be found in Appendix A.

When determining the values of \mathbf{W}_1 and \mathbf{W}_2 we would like to avoid utilizing the prior scan in the reconstruction process if the assumption of similarity between consecutive scans does not hold. More specifically, we design \mathbf{W}_1 and \mathbf{W}_2 to achieve the following goals:

1. Convergence to CS-MRI (1) if the assumption of similarity between consecutive scans is not valid (i.e.: $w_1^i \rightarrow 1$ and $w_2^i \rightarrow 0$ if \mathbf{x} and \mathbf{x}_0 are significantly different in both image and wavelet domains).
2. Relaxing the demand for sparsity of $\Psi\mathbf{x}$ in regions where $\Psi\mathbf{x}_0$ is not sparse and the similarity assumption between $\Psi\mathbf{x}$ and $\Psi\mathbf{x}_0$ is valid. (i.e.: $w_1^i \rightarrow 0$ as $[\|\Psi\mathbf{x}_0\|]_i$ grows and images are similar in the transform domain)
3. Relaxing the demand for sparsity of $(\mathbf{x} - \mathbf{x}_0)$ in regions where the similarity assumption between \mathbf{x} and \mathbf{x}_0 is not valid (i.e.: $w_2^i \rightarrow 0$ as $[\|\mathbf{x} - \mathbf{x}_0\|]_i$ grows).

To obtain the goals above, we first sample N_k \mathbf{k} -space samples randomly and reconstruct $\hat{\mathbf{x}}$, which is the estimation of \mathbf{x} , by solving (5) with $\mathbf{W}_1 = \mathbf{I}$ and $\mathbf{W}_2 = \mathbf{0}$. We then sample additional N_k samples and solve (5) where the elements of the matrices are chosen as follows:

$$w_1^i = \begin{cases} 1, & \frac{[\|\Psi(\hat{\mathbf{x}} - \mathbf{x}_0)\|]_i}{1 + [\|\Psi(\hat{\mathbf{x}} - \mathbf{x}_0)\|]_i} > \epsilon_1 \\ \frac{1}{1 + [\|\Psi\mathbf{x}_0\|]_i}, & otherwise \end{cases} \quad (6)$$

$$w_2^i = \frac{1}{1 + [\|\hat{\mathbf{x}} - \mathbf{x}_0\|]_i} \quad (7)$$

where $[\cdot]_i$ denotes the i th element of the vector in brackets and ϵ_1 is a threshold for defining similarity in the sparse transform domain. This process is repeated until a sufficient number of samples has been obtained for adequate recovery. This iterative approach allows exploitation of temporal similarity, when it exists, and prevents degradation of image quality if the consecutive scans are significantly different.

Incorporating adaptive sampling into the longitudinal MRI problem is obtained via adaptive design of the N_k sampling locations at each iteration. It is well known that reconstruction results highly depend with sampling trajectories in \mathbf{k} -space domain. For instance, random sampling is one of the requirement of CS and one should be undersampling less near the \mathbf{k} -space origin and more in the periphery of \mathbf{k} -space (Tsai and Nishimura, 2000;

Lustig et al., 2007). A common sampling scheme is variable density random undersampling (VDS), which can be implemented by choosing samples randomly with sampling density scaling according to a power of distance from the origin.

For simplicity, we assume that 2D Cartesian sampling is used, and the N_k sampling locations consist of rows sampling in the \mathbf{k} -space domain. To utilize VDS in 2D Cartesian sampling we define the discrete polynomial distribution as:

$$f_{VD}(k_y) = \frac{(1 - \frac{2}{n}|k_y|)^p}{\sum_{k_y} (1 - \frac{2}{n}|k_y|)^p} \quad (8)$$

where $-\frac{n}{2} < k_y \leq \frac{n}{2}$ denotes the \mathbf{k} -space coefficients in the phase encoding direction and p is the power distance from the origin.

VDS is used as the probability density function (pdf) for random sampling in many cases where the real distribution of the data is a-priori unknown. However, in longitudinal studies we may rely on the reference scan data distribution, if scans are similar. Inspired by Chen et al. (Chen et al., 2014), our adaptive approach will converge to random sampling according to the reference scan data pdf if it is similar to the follow-up scan, and to polynomial pdf otherwise. Therefore, samples in our approach are taken randomly using the following pdf:

$$f_S(k_y) = \gamma f_B(k_y) + (1 - \gamma) f_{VD}(k_y) \quad (9)$$

where f_B is the pdf of the baseline's phase encode lines' energy, defined as:

$$f_B(k_y) = \frac{g_B(k_y)}{\sum_{k_y} g_B(k_y)} \quad , \quad g_B(k_y) = \sum_{i \in k_y} [|\mathbf{F}\mathbf{x}_0|]_i \quad (10)$$

\mathbf{F} indicates the $N \times N$ Fourier matrix, $[\cdot]_i$ denotes the i th element of the vector in brackets and γ is the fidelity we give to the similarity between the current and the previous scan. Since \mathbf{W}_2 can serve as a good approximation for this similarity, γ is computed as its mean over the main diagonal: $\gamma = \frac{1}{N} \sum_{i=1}^N w_2^i$.

A diagram presenting the major differences between CS-MRI, TCS-MRI and the proposed method is shown in Fig. 3. The details of the proposed approach are summarized in Algorithm 1. This scheme for longitudinal adaptive-weighted compressed sensing is coined hereinafter LACS-MRI

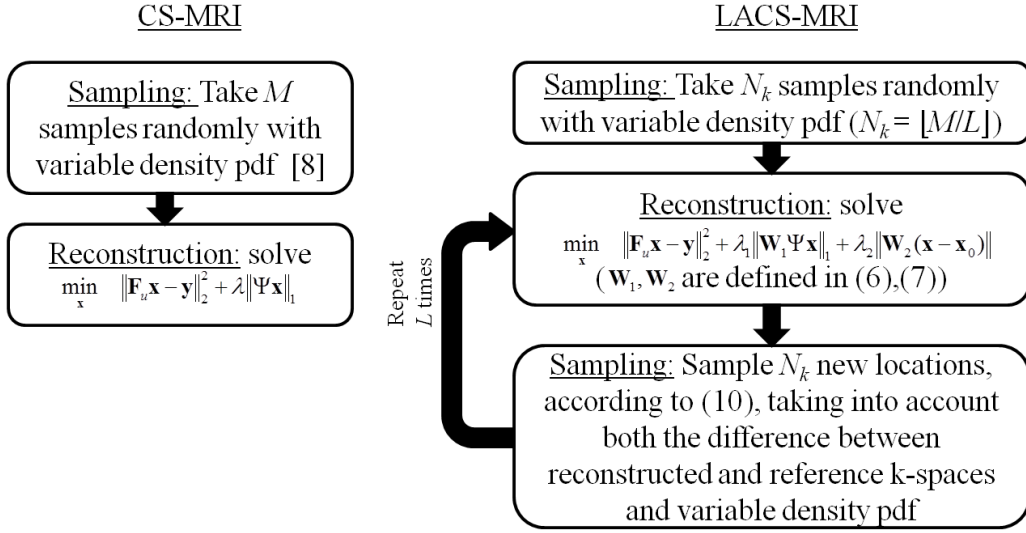


Figure 3: High-level diagram showing the main steps in the CS-MRI approach (left) and our proposed adaptive approach (right). Both approaches acquire M \mathbf{k} -space samples. However, in LACS-MRI only a small portion of the samples is taken from a pure variable density pdf, in the first iteration. The rest of the samples are taken iteratively, taking into account both the difference between the \mathbf{k} -spaces of the reconstructed image, \mathbf{x} , and the previous image in the time series, \mathbf{x}_0 and the variable density pdf.

(Longitudinal Adaptive Compressed Sensing MRI).

Algorithm 1 Adaptive-weighted temporal CS MRI (LACS-MRI)

Input:

Number of \mathbf{k} -space samples acquired at each iteration: N_k ;

Number of iterations: L ;

Image from earlier time-point: \mathbf{x}_0 ;

Output: Estimated image: $\hat{\mathbf{x}}$

Initialize:

$\mathbf{y} = \mathbf{0}$; $\mathbf{F}_u = \mathbf{0}$; $S = \emptyset$; $\mathbf{W}_1 = \mathbf{I}$; $\mathbf{W}_2 = \mathbf{0}$;

Randomly define N_k \mathbf{k} -space sampling locations: $S^{(1)} = \{s_1, s_2, \dots, s_{N_k}\}$ according to (8)

Sampling and reconstruction:

for $l = 1$ to L **do**

$S \leftarrow S \cup S^{(l)}$

Define undersample operator: $\mathbf{F}_u^{(l)}(i, j) = \begin{cases} \mathbf{F}(i, j), & i \in S \\ 0, & i \notin S \end{cases}$

Sample: $\mathbf{y}^{(l)} = \mathbf{F}_u^{(l)} \mathbf{x}$

Update: $\mathbf{y} = \mathbf{y} + \mathbf{y}^{(l)}$; $\mathbf{F}_u = \mathbf{F}_u + \mathbf{F}_u^{(l)}$

Weighted reconstruction:

$\hat{\mathbf{x}} = \min_{\mathbf{x}} \|\mathbf{F}_u \mathbf{x} - \mathbf{y}\|_2^2 + \lambda_1 \|\mathbf{W}_1 \Psi \mathbf{x}\|_1 + \lambda_2 \|\mathbf{W}_2 (\mathbf{x} - \mathbf{x}_0)\|_1$

Adaptive sampling:

Update \mathbf{W}_1 and \mathbf{W}_2 according to (6) and (7)

Use pdf in (9) to randomly define N_k new sampling locations, $S^{(l+1)}$

end for

3. Experimental results

3.1. Experimental settings

Our experiments consist of repeated scans of pomelo and patients with OPG and GBM. The patients with OPG were scanned with a GE Signa 1.5T HDx scanner and the pomelo and GBM experiments were performed on a GE Signa 3T HDXT scanner. In our experiments, partial \mathbf{k} -space acquisition was obtained by down-sampling, in a software environment, a fully sampled \mathbf{k} -space. All CS reconstructions were implemented in Matlab (The MathWorks, Natick, MA). We compare our approach (LACS-MRI) with two non-adaptive

schemes, CS-MRI and temporal CS-MRI (TCS MRI). CS-MRI is described in (Lustig et al., 2007) and TCS-MRI takes into account the knowledge of the prior scan in the time sequence, by solving (2) for image reconstruction.

In our experiments we used the Daubechies 4 wavelet transform. Reconstructions based on non-adaptive sampling (CS-MRI and TCS-MRI) were obtained with variable density undersampling, where samples were taken randomly according to the pdf in (8) with $p = 4$. In 2D Cartesian sampling 5% of the phase encode lines, located in its center were acquired in full. In 3D Cartesian sampling 1% of the phase encode plane was acquired in full. For LACS-MRI we used the same variable density random pattern for the first iteration, while subsequent samples were taken according to Algorithm 1.

LACS-MRI and TCS-MRI ℓ_1 -minimization problems were solved in their Lagrangian form using the FISTA algorithm, described in Appendix A. CS-MRI was tested both with our FISTA-based implementation of solving (1) and with the non-linear conjugate sub-gradient algorithm as described in (Lustig et al., 2007), which adds a Total Variation (TV) (Tsaig and Donoho, 2006) penalty to (1), where the best results (in terms of resolution improvement) are shown. The threshold for defining similarity in the sparse transform domain was set to $\epsilon_1 = 0.1$. In all experiments, different values of λ_1, λ_2 in the range of $[0.001, 0.9]$ were examined, and the best result is shown for each reconstruction algorithm.

For quantitative evaluation, the Signal-to-Noise ration (SNR) is computed for each reconstruction result, as: $SNR = 10\log_{10}(\sigma_{\mathbf{x}}/V_s)$, where $\sigma_{\mathbf{x}}$ denotes the variance of the values in \mathbf{x} and V_s is the Mean Square Error (MSE) between the original image, \mathbf{x} and the reconstructed image, $\hat{\mathbf{x}}$. Note that in some cases clinical decisions are based on subtle changes between the baseline and the follow-up scans, that are not reflected in the SNR. Therefore, results are presented both visually and quantitatively.

3.2. 2D Cartesian Sampling of Static Pomelo

First, we acquired T1-weighted pomelo image using a SE sequence (matrix: 256×256 , res= $1mm$, 35 slices with $6mm$ thickness and no gap, $TR/TE = 600/8ms$, flip angle= 90°). Then, we injected a contrast agent into the pomelo in order to create structural changes in the pomelo without changing its spatial orientation. We then repeated the scan with the same acquisition parameters to obtain a post-contrast T1-weighted (T1c) image. As a result,

we obtained two pomelo images, spatially matched, that simulate a baseline scan and a follow-up scan that consists of changes from the baseline scan.

The aim of the simulation is to examine the performance of utilizing sparsity in both the wavelet and temporal domains with adaptive sampling for longitudinal scans, with LACS-MRI, in the absence of external artifacts such as miss-registration errors or movements during acquisition.

We performed 2D reconstruction with LACS-MRI, CS-MRI and TCS-MRI. We set the number of samples acquired at the first iteration for LACS-MRI to $N_k = 8$ lines. Results are shown with corresponding acceleration factors of 4, 6.4, and 10.6.

The SNR values of the different reconstruction results are shown in Table 1. Figure 4 shows the baseline and follow-up pomelo images and the reconstruction results. As expected, reconstruction results improve as the acceleration ratio decreases, for all methods. The major differences between the baseline and follow-up scans consist of two enhancing regions (marked in arrows), due to the injection of a contrast agent before the acquisition of the follow-up scan.

In terms both image resolution and SNR, LACS-MRI outperforms TCS-MRI and CS-MRI, by exhibiting significantly improved recovery of the image at 4-fold acceleration, which also allows to identify changes versus the baseline scans, i.e. the two enhanced areas. Although both TCS-MRI and LACS-MRI utilize temporal similarity in the reconstruction process, this experiment emphasizes the advantage of embedding weighted-CS and adaptive sampling. Together with the weighting mechanism, the sampling locations (shown in the bar next to each image) which were chosen adaptively by LACS-MRI, lead to improved reconstruction results versus the pure random sampling used in CS-MRI and TCS-MRI.

Table 1: Comparisons of the SNR (db), Pomelo experiment

Acceleration factor	CS-MRI	TCS-MRI	LACS-MRI
10.6	2.2468	2.9052	3.6107
6.4	2.9139	7.0814	13.8731
4	4.1401	10.9464	18.2111

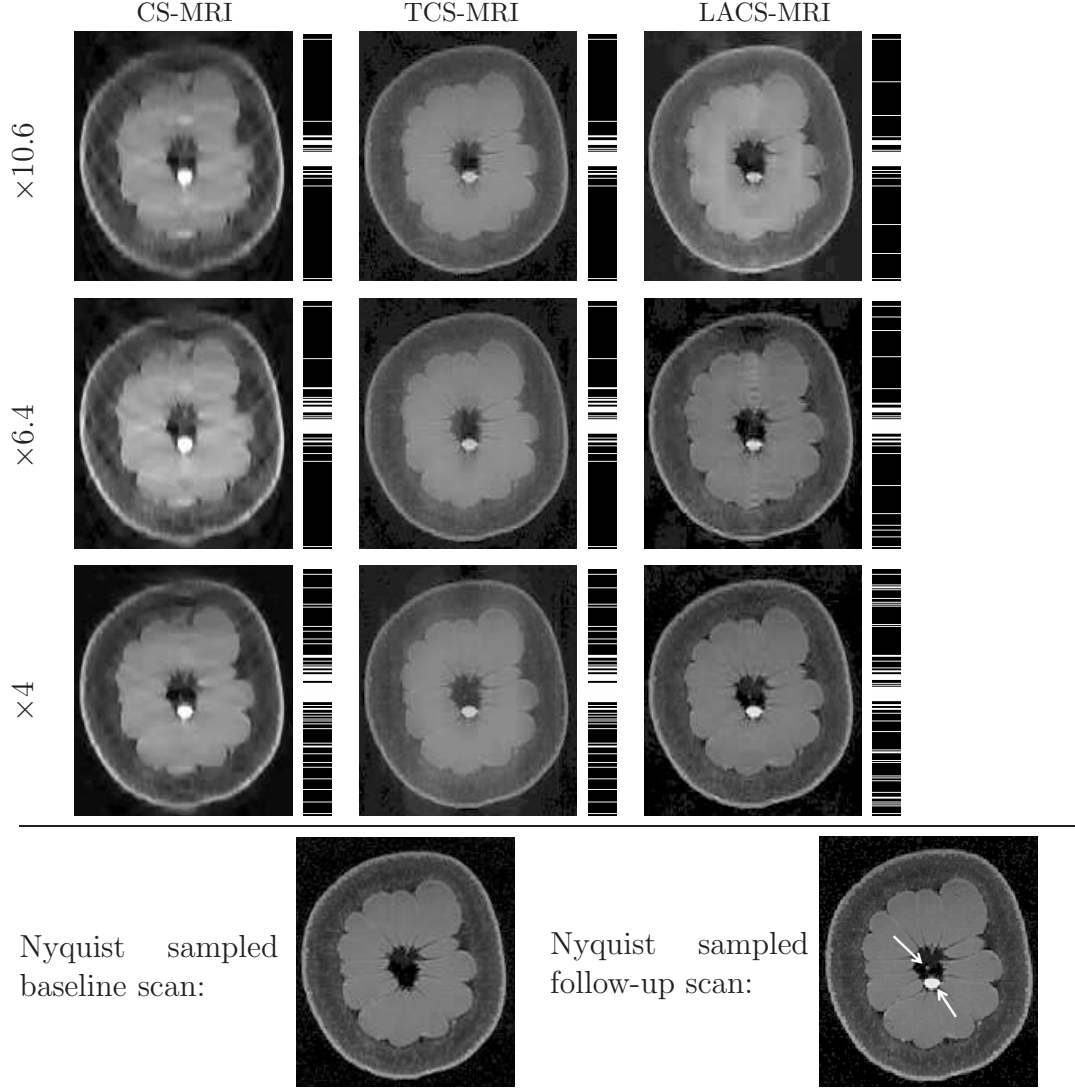


Figure 4: Pomelo experiment: The bottom row shows the scans of a pomelo before (left) and after (right) contrast agent injection, simulating a baseline and a follow-up scan. The major changes are seen in the follow-up scan as two enhancing regions, marked by arrows on the Nyquist sampled follow-up scan. Results of CS-MRI, TCS-MRI and LACS-MRI are presented at acceleration factors of 4, 6.4 and 10.6. The bar next to each image shows sampled phase encode lines under each scheme. It can be seen that LACS-MRI outperforms CS-MRI and TCS-MRI, and exhibits significantly improved resolution at acceleration factor of 4.

3.3. 3D Fast Spoiled Gradient Echo Brain Imaging

Applying CS for 3D imaging allows undersampling in the 2D phase encode plane, thereby obtaining better performance than applying 2D CS slice by slice. We used two retrospectively acquired scans of a patient with OPG, where scans were acquired in an interval of six months. We used contrast enhanced 3D T1-weighted FSPGR sequence (matrix: $512 \times 512 \times 46$, res = $0.47mm$, slice= $1.7mm$, TI/TR/TE= $450/14.5/6.3ms$, flip angle= 20°).

We rigidly registered the later scan to the former scan and then under-sampled the 3DFT trajectory with corresponding acceleration factors of 5, 10 and 16.6 (20%, 10% and 6% of the \mathbf{k} -space). For LACS-MRI we begin with variable density random undersampling of 2% of the \mathbf{k} -space and acquire additional 2% of the \mathbf{k} -space at each iteration as described in Algorithm 1.

Table 2 shows the SNR values of the different reconstruction results. Figure 5 shows the reconstruction results at 5,10 and 16.6-fold acceleration of a patient with OPG. Both TCS-MRI and LACS-MRI exhibit almost no loss of information at 10-fold acceleration. Similar results are obtained with CS-MRI only at 5-fold acceleration.

This experiment shows that thanks to the ability to under-sample the 2D phase encode plane, the advantage of temporal similarity exploitation is emphasized. Therefore, LACS-MRI allows shortening the scanning time by a factor of 10, with no significant loss of information in this case.

Table 2: Comparisons of the SNR (db), 3D FSPGR experiment

Acceleration factor	CS-MRI	TCS-MRI	LACS-MRI
16.6	11.5093	20.4286	24.8350
10	22.9917	24.3437	27.3621
5	25.4494	28.0273	29.9281

3.4. 2D Fast Spin-Echo Brain Imaging of Rapidly Changing Tumor

To examine the performance of our approach with brain MRI data when the assumptions of similarity between consecutive scans is not valid, we used retrospectively acquired data of a patient with GBM. The patient was scanned twice within an interval of five months, and exhibited changes between scans that occupy more than 50% of the brain region. We used T2-weighted FSE sequence (matrix: 512×512 res = $0.47mm$, 36 slices with

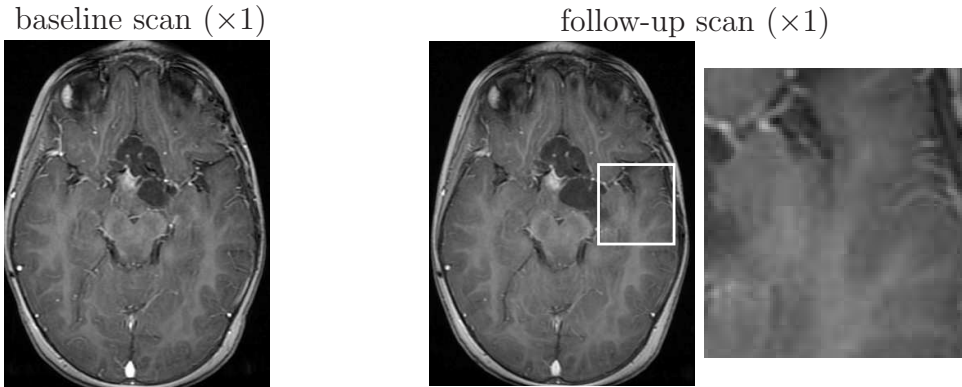
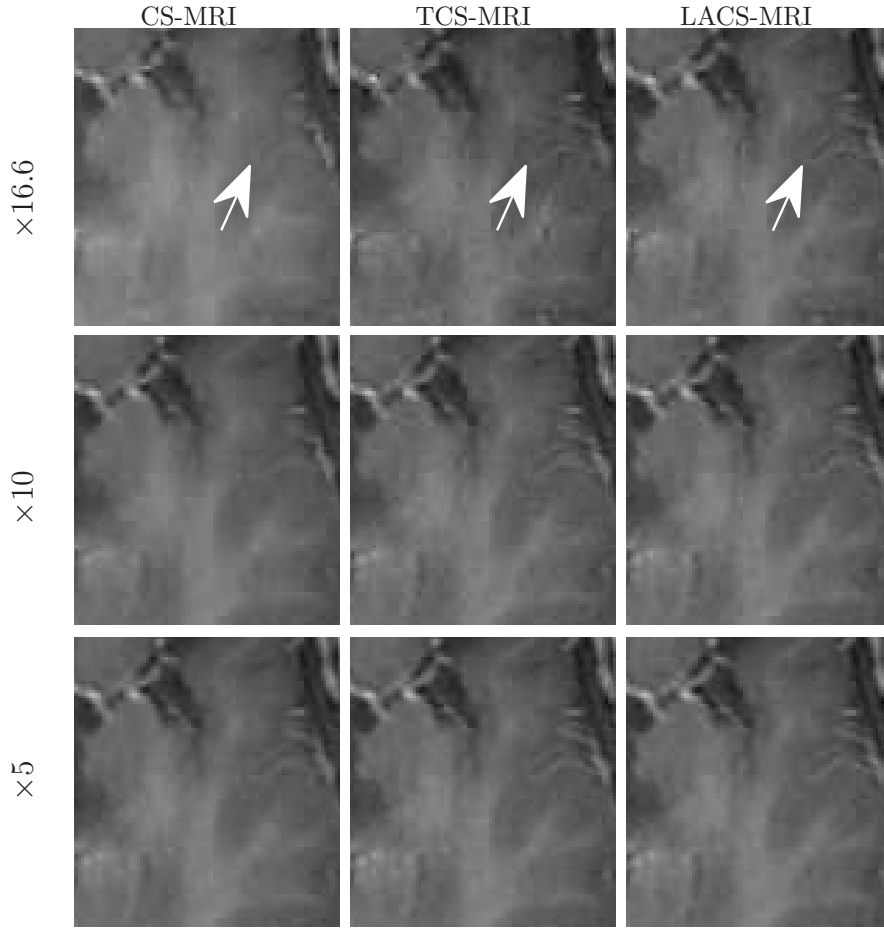


Figure 5: 3D FSPGR results. While CS-MRI and TCS-MRI exhibit artifacts at 16.6-fold acceleration, LACS-MRI exhibits improved resolution (pointed by arrows). At 10-fold acceleration, TCS-MRI and LACS-MRI exhibit similar satisfactory performance, while CS-MRI exhibits some reconstruction artifacts. At 5-fold acceleration all method exhibit almost no loss of information with slightly better performance obtained by LACS-MRI.

4mm thickness and no gap, TR/TE=3500/113ms, echo-train length=24, flip angle=90°). We registered the follow-up scan to the baseline scan and examined the results of LACS-MRI ($N_k = 16$), CS-MRI and TCS-MRI with acceleration factors of 4, 6.4, and 10.6.

Table 3 shows the SNR values for different reconstructions and Figure 6 shows reconstruction results visually, at acceleration factor of 4 (25% of the \mathbf{k} -space). In this case, there are major changes between the baseline and the follow-up scans due to therapy response. As a result, TCS-MRI exhibits poor performance in the vicinity of the changing tumor, since it is partially based on similarity between the consecutive scans, an assumption which is not valid in this case.

LACS-MRI, however, converges to a result which is similar to CS-MRI. This is obtained thanks to the adaptive sampling and the weighting mechanism embedded in LACS-MRI, which reduces the weight given to the similarity to prior scan in the reconstruction process, if such a similarity does not exist.

Table 3: Comparisons of the SNR (db), 2D FSE experiment, major temporal changes changes.

Acceleration factor	CS-MRI	TCS-MRI	LACS-MRI
10.6	8.2324	7.4092	8.9705
6.4	9.1760	8.2584	9.7180
4	20.1972	18.1775	20.6306

4. Discussion

4.1. Reproducing image orientation in longitudinal studies

The exploitation of temporal similarity in longitudinal studies assumes that the past scan and the follow-up scan being acquired are spatially matched. In our experiments, we worked with retrospectively acquired data and rigidly registered the later scan to the former scan. Note that our method exhibits reliable performance even when minor registration errors exist (as can be seen in the difference images in Fig. 6), thanks to the similarity of adjacent pixels in MRI.

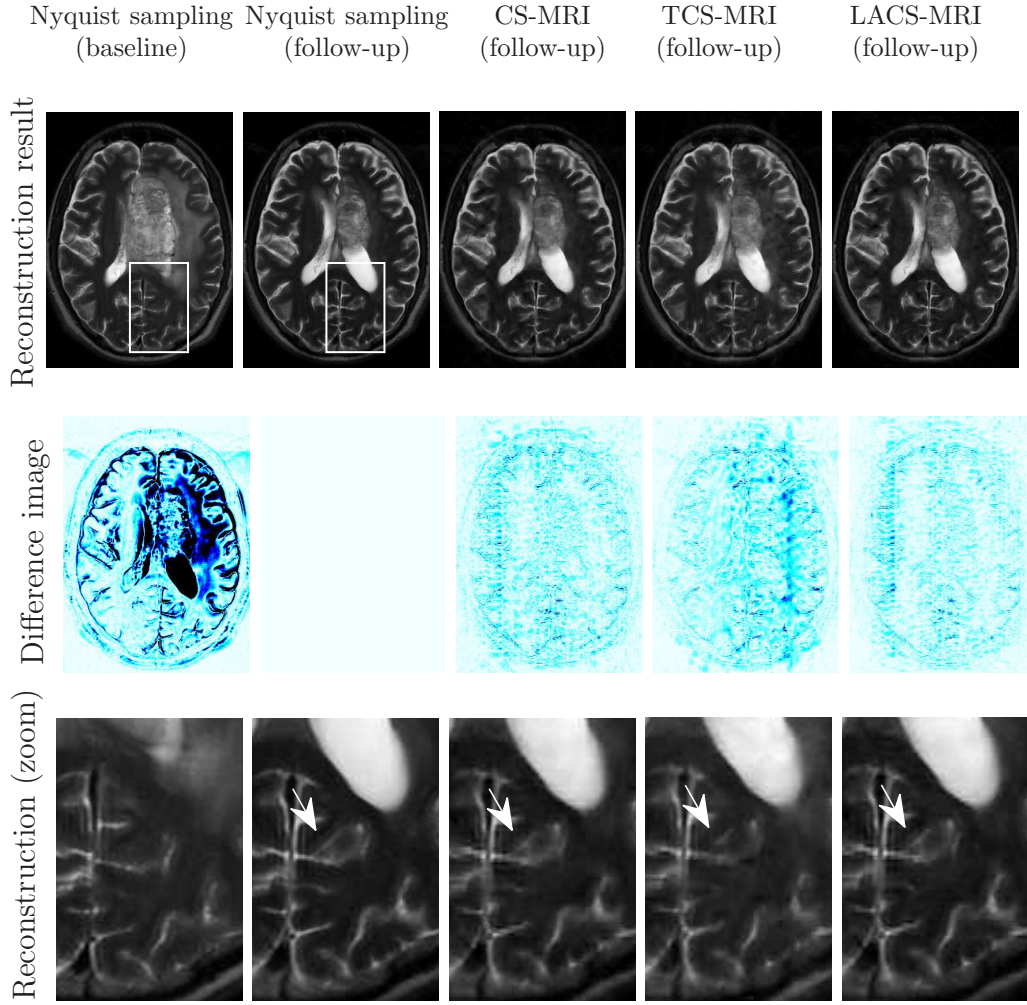


Figure 6: 2D FSE brain imaging results when similarity between baseline and follow-up is minimal. The leftmost column shows the baseline scan used as \mathbf{x}_0 for TCS-MRI and LACS-MRI. The difference image between the baseline and the follow-up scans shows substantial changes due to rapid tumor changes. The last row shows an enlargement of the white rectangle. LACS-MRI and CS-MRI exhibit similar results, where TCS-MRI exhibits sub-optimal results in the changes regions, due to its wrong assumption of substantial between the baseline and the follow-up scans.

The practical implementation of our method for prospective acquisition of follow-up scans requires reproducing the past scan’s slice positions for the scan being acquired. This spatial matching is currently offered as a feature by some MRI vendors (McMillan et al., 2010), and is based on several anatomical landmark. As previously noted, our method is expected to overcome minor matching errors which might be produced by these tools thanks to fact that adjacent pixels have similar values in many MRI applications.

An additional practical solution could utilize the adaptive sampling mechanism. Partially sampled data can be used to determine the spatial orientation of the patient vs. the reference image, during acquisition. This approach have been tested to compensate motions during imaging (Lingala et al., 2011; Feng et al., 2013) and can be utilized for the longitudinal scanning case.

The applicability of the proposed method to other regions outside of the brain, such as abdominal MRI is more complicated as it may require non-rigid registration. Therefore, this paper focuses on the application of CS for longitudinal brain studies, while the implementation for regions outside of the brain is left for future research.

4.2. Grey Level Intensity Differences

The exploitation of temporal similarity is performed by utilizing the fact that the difference between the baseline and the follow-up scans is sparse, and consists changes in anatomy or pathology. However, changes between baseline and follow-up scans may be the result of other factors, such as acquisition parameters and field inhomogeneity. In this work, we normalized the grey level intensity values of the scans to match the same scale, in order to minimize the effect of external factors on changes between the scans. This normalization was sufficient for producing the results presenting in this paper. In prospective scanning, the normalization coefficients can be determined iteratively, during the sampling and reconstruction process.

In the special case of longitudinal studies, scans are in many cases acquired in the same scanning site with the same scanning protocol, to minimize the effect of external parameters on the resulted clinical follow-up. When the baseline and follow-up scans are acquired with different acquisition parameters on different systems, we can still exploit the structural similarity between the baseline and the follow-up scans for rapid acquisition. While this extension is not in the scope of this paper, the reader is referred to the works of Bilgic et al. (Bilgic et al., 2011) and Huang et al. (Huang et al., 2012)

who utilize the structural similarity between various MRI sequences for rapid scanning.

4.3. Computational Complexity

Fast algorithms for solving ℓ_1 minimization problems have gained much attention recently. Besides FISTA (Beck and Teboulle, 2009), used in our experiments, we find NESTA (Becker et al., 2011), SALSA (Afonso et al., 2010), C-SALSA (Afonso et al., 2011), SPGL1 (Van Den Berg and Friedlander, 2008) among other approaches that report improved convergence time and have not been explored in this work.

Fast convergence time is important in our adaptive sampling approach, that requires solving ℓ_1 minimization problem to decide on the sampling locations for the next iteration. In a Matlab (The MathWorks, Natick, MA) implementation, each ℓ_1 minimization for 256×256 brain image requires approximately 35 seconds.

While our implementation of FISTA at present does not attain the high rates required for solving ℓ_1 minimization for real-time applications, we expect a significant reduction in the reconstruction time by code optimization. Examining new approaches for ℓ_1 minimization, algorithmic simplifications, combined with massively parallel digital computation could allow our framework to be used in the future in order to allow the adaptive sampling mechanism operate during MRI scanning.

5. Conclusions

Repeated scans constitute a substantial portion of MRI scanning today, mainly to track changes in pathologies and to monitor treatment efficacy. We presented LACS MRI based on adaptive sampling and weighted-CS for rapid MR imaging of longitudinal studies. We demonstrated experimental verification of several implementations for 2D and 3D Cartesian imaging. We showed that the temporal sparsity of longitudinal MR images can be exploited to significantly reduce scan time of follow-up scans, or alternatively, improve their resolution.

We demonstrated that unlike other CS-MRI applications, sparsity in the temporal domain is not guaranteed in longitudinal studies. We showed that our method provides almost no loss of information at 10-fold acceleration of 3D brain scans, when there is substantial similarity between baseline and follow-up scan. Moreover, our method adapts to a scenario in which there is

substantial difference between the scans and results converge to state-of-the-art CS-MRI in this case.

LACS-MRI can play a major part in applications that consist of patient's disease follow-up and changes monitoring. This could be a first step towards utilizing the huge amount of data in picture archiving and communication systems (PACS) to speed-up MRI.

Appendix A. Fast Iterative Shrinkage-Thresholding Algorithm for LACS-MRI

LACS-MRI poses an unconstrained problem in so-called Lagrangian form:

$$\min_{\mathbf{x}} \quad \|\mathbf{F}_u \mathbf{x} - \mathbf{y}\|_2^2 + \lambda_1 \|\mathbf{W}_1 \Psi \mathbf{x}\|_1 + \lambda_2 \|\mathbf{W}_2 (\mathbf{x} - \mathbf{x}_0)\|_1. \quad (\text{A1})$$

We solve (A1) with Fast Iterative Shrinkage-Thresholding (FISTA) (Beck and Teboulle, 2009). Originally, FISTA was introduced to solve the following problem:

$$\min_{\mathbf{x}} \quad \|\mathbf{A} \mathbf{x} - \mathbf{y}\|_2^2 + \lambda \|\mathbf{x}\|_1. \quad (\text{A2})$$

Recently, Tan et al. (Tan et al., 2014) proposed a FISTA-based that allows for weighted- ℓ_1 of the form:

$$\min_{\mathbf{x}} \quad \|\mathbf{A} \mathbf{x} - \mathbf{y}\|_2^2 + \lambda \|\mathbf{D}^* \mathbf{x}\|_1 \quad (\text{A3})$$

Their algorithm, coined SFISTA, is described as Algorithm 1 in (Tan et al., 2014). Based on (Tan et al., 2014) we define the following:

$$f(\mathbf{x}) = \mathbf{F}_u \mathbf{x} - \mathbf{y} \quad (\text{A4})$$

$$g_{1\mu}(\mathbf{W}_1 \Psi \mathbf{x}) = \min_{\mathbf{u}} \left\{ \lambda_1 \|\mathbf{u}\|_1 + \frac{1}{2\mu} \|\mathbf{u} - \mathbf{W}_1 \Psi \mathbf{x}\|_2^2 \right\} \quad (\text{A5})$$

$$g_{2\mu}(\mathbf{W}_2 (\mathbf{x} - \mathbf{x}_0)) = \min_{\mathbf{u}} \left\{ \lambda_2 \|\mathbf{u}\|_1 + \frac{1}{2\mu} \|\mathbf{u} - \mathbf{W}_2 (\mathbf{x} - \mathbf{x}_0)\|_2^2 \right\} \quad (\text{A6})$$

Extending SFISTA to solve (A1) results in the following algorithm:

SFISTA algorithm for LACS-MRI
Input:

\mathbf{k} -space measurements: \mathbf{y} ;

Sparsifying transform operator: Ψ

An $N \times N$ undersampling operator in the k-space domain: \mathbf{F}_u

Image from earlier time-point: \mathbf{x}_0 ;

Tuning constants: $\lambda_1, \lambda_2, \mu$

An upper bound: $L \geq \|\mathbf{F}_u\|_2^2 + \frac{\|\mathbf{W}_1\Psi\|_2^2 + \|\mathbf{W}_2\|_2^2}{\mu}$

Output: Estimated image: $\hat{\mathbf{x}}$

Initialize:

$$\mathbf{x}_0 = \mathbf{z}_1 = \mathbf{F}_u^* \mathbf{y}, t_1 = 1$$

Iterations:

Step k: ($k \geq 1$) Compute

$$\nabla f(\mathbf{z}_k) = \mathbf{F}_u^* (\mathbf{F}_u \mathbf{z}_k - \mathbf{y})$$

$$\nabla g_{1\mu}(\mathbf{W}_1 \Psi \mathbf{x}_{k-1}) = \frac{1}{\mu} \mathbf{W}_1 \Psi^* (\mathbf{W}_1 \Psi \mathbf{x}_{k-1} - \Gamma_{\lambda_1 \mu}(\mathbf{W}_1 \Psi \mathbf{x}_{k-1}))$$

$$\nabla g_{2\mu}(\mathbf{W}_2(\mathbf{x}_{k-1} - \mathbf{x}_0)) = \frac{1}{\mu} \mathbf{W}_2 (\mathbf{W}_2(\mathbf{x}_{k-1} - \mathbf{x}_0) - \Gamma_{\lambda_2 \mu}(\mathbf{W}_2(\mathbf{x}_{k-1} - \mathbf{x}_0)))$$

$$\mathbf{u}_k = \mathbf{z}_k - \frac{1}{L} (\nabla f(\mathbf{z}_k) + \nabla g_{1\mu}(\mathbf{W}_1 \Psi \mathbf{x}_{k-1}) + \nabla g_{2\mu}(\mathbf{W}_2(\mathbf{x}_{k-1} - \mathbf{x}_0)))$$

$$t_{k+1} = \frac{1 + \sqrt{1 + 4t_k^2}}{2}$$

$$\mathbf{x}_k = \operatorname{argmin}\{H_\mu(\mathbf{x}) : \mathbf{x} = \mathbf{u}_k, \mathbf{x}_{k-1}\}$$

$$\mathbf{z}_{k+1} = \mathbf{x}_k + \frac{t_k}{t_{k+1}} (\mathbf{u}_k - \mathbf{x}_k) + \frac{t_k - 1}{t_{k+1}} (\mathbf{x}_k - \mathbf{x}_{k-1})$$

where the notation $\|\cdot\|_2$ for matrices denotes the largest singular value, and $\Gamma_{\lambda\mu}(\mathbf{z})$ is the soft shrinkage operator, which operates element-wise on \mathbf{z} and defined as (for complex valued z_i):

$$\Gamma_{\lambda\mu}(z_i) = \begin{cases} \frac{|z_i| - \lambda\mu}{|z_i|} z_i, & |z_i| > \lambda\mu \\ 0, & \text{otherwise} \end{cases} \quad (\text{A7})$$

and:

$$H_\mu(\mathbf{x}) = \|\mathbf{F}_u \mathbf{x} - \mathbf{y}\|_2^2 + g_{1\mu}(\mathbf{W}_1 \Psi \mathbf{x}) + g_{2\mu}(\mathbf{W}_2(\mathbf{x} - \mathbf{x}_0)) \quad (\text{A8})$$

The algorithm above minimizes (A1), where the trade-off between the two sparsity assumptions is controlled by the ratio between λ_1 and λ_2 , via $\Gamma(\cdot)$, and the overall convergence is controlled by μ . Typical values for λ_1 and λ_2 are in the range of $[0.001, 0.9]$. The value of μ usually depends with the values of λ_1 and λ_2 and is in the range of $[10^{-9}, 100]$. The value of $\mu = 10^{-3}(\frac{\lambda_1 + \lambda_2}{2})^{-1}$

was used in our experiments. The number of iterations varies with different objects, problem size, accuracy and undersampling. Examples in this paper required between 30 and 50 iterations.

Acknowledgements

The authors wish to thank the Gilbert Israeli Neurofibromatosis Center (GINFC) for providing the real data and supporting the medical part of the paper. This research was supported by the Ministry of Science and Technology, Israel.

References

References

- Afonso, M.V., Bioucas-Dias, J.M., Figueiredo, M., 2011. An augmented lagrangian approach to the constrained optimization formulation of imaging inverse problems. *Image Processing, IEEE Transactions on* 20, 681–695.
- Afonso, M.V., Bioucas-Dias, J.M., Figueiredo, M.A., 2010. Fast image recovery using variable splitting and constrained optimization. *Image Processing, IEEE Transactions on* 19, 2345–2356.
- Arias-Castro, E., Candes, E.J., Davenport, M.A., 2013. On the fundamental limits of adaptive sensing. *Information Theory, IEEE Transactions on* 59, 472–481.
- Beck, A., Teboulle, M., 2009. A fast iterative shrinkage-thresholding algorithm for linear inverse problems. *SIAM Journal on Imaging Sciences* 2, 183–202.
- Becker, S., Bobin, J., Candès, E.J., 2011. NESTA: a fast and accurate first-order method for sparse recovery. *SIAM Journal on Imaging Sciences* 4, 1–39.
- Bilgic, B., Goyal, V.K., Adalsteinsson, E., 2011. Multi-contrast reconstruction with bayesian compressed sensing. *Magnetic Resonance in Medicine* 66, 1601–1615.

- Candès, E.J., 2006. Compressive sampling, in: Proceedings of the International Congress of Mathematicians: Madrid, August 22-30, 2006: invited lectures, pp. 1433–1452.
- Candès, E.J., Wakin, M.B., Boyd, S.P., 2008. Enhancing sparsity by reweighted ℓ_1 minimization. *Journal of Fourier analysis and applications* 14, 877–905.
- Cao, Y., Levin, D.N., 1993. Feature-recognizing MRI. *Magnetic resonance in medicine* 30, 305–317.
- Cao, Y., Levin, D.N., Yao, L., 1995. Locally focused MRI. *Magnetic resonance in medicine* 34, 858–867.
- Chen, G., Tang, J., Leng, S., 2008. Prior image constrained compressed sensing (piccs): a method to accurately reconstruct dynamic ct images from highly undersampled projection data sets. *Medical physics* 35, 660–663.
- Chen, Y., Bhojanapalli, S., Sanghavi, S., Ward, R., 2014. Completing any low-rank matrix, provably. *arXiv preprint*. *arXiv preprint arXiv:1306.2979* .
- Daubechies, I., et al., 1992. Ten lectures on wavelets. volume 61. SIAM.
- Donoho, D., Tsai, Y., 2008. Fast solution of ℓ_1 -norm minimization problems when the solution may be sparse. *Information Theory, IEEE Transactions on* 54, 4789–4812.
- Donoho, D.L., 2006. Compressed sensing. *Information Theory, IEEE Transactions on* 52, 1289–1306.
- Eldar, Y.C., Kutyniok, G., 2012. Compressed sensing: theory and applications. Cambridge University Press.
- Feng, L., Grimm, R., Block, K.T., Chandarana, H., Kim, S., Xu, J., Axel, L., Sodickson, D.K., Otazo, R., 2013. Golden-angle radial sparse parallel MRI: Combination of compressed sensing, parallel imaging, and golden-angle radial sampling for fast and flexible dynamic volumetric MRI. *Magnetic Resonance in Medicine* .

- Fessler, J.A., Clinthorne, N.H., Rogers, W., 1992. Regularized emission image reconstruction using imperfect side information. *Nuclear Science, IEEE Transactions on* 39, 1464–1471.
- Friedlander, M.P., Mansour, H., Saab, R., Yilmaz, Ö., 2012. Recovering compressively sampled signals using partial support information. *Information Theory, IEEE Transactions on* 58, 1122–1134.
- Gamper, U., Boesiger, P., Kozerke, S., 2008. Compressed sensing in dynamic MRI. *Magnetic Resonance in Medicine* 59, 365–373.
- Gao, Y., Reeves, S.J., 2000. Optimal k-space sampling in MRSI for images with a limited region of support. *Medical Imaging, IEEE Transactions on* 19, 1168–1178.
- Haldar, J.P., Hernando, D., Song, S., Liang, Z., 2008. Anatomically constrained reconstruction from noisy data. *Magnetic Resonance in Medicine* 59, 810–818.
- Haupt, J., Castro, R.M., Nowak, R., 2011. Distilled sensing: Adaptive sampling for sparse detection and estimation. *Information Theory, IEEE Transactions on* 57, 6222–6235.
- Haupt, J., Nowak, R., Castro, R., 2009. Adaptive sensing for sparse signal recovery, in: *Digital Signal Processing Workshop and 5th IEEE Signal Processing Education Workshop, 2009. DSP/SPE 2009. IEEE 13th, IEEE*. pp. 702–707.
- Hero, A., Piramuthu, R., Fessler, J.A., Titus, S.R., 1999. Minimax emission computed tomography using high-resolution anatomical side information and b-spline models. *Information Theory, IEEE Transactions on* 45, 920–938.
- Hu, X., Levin, D.N., Lauterbur, P.C., Spraggins, T., 1988. Slim: Spectral localization by imaging. *Magnetic resonance in medicine* 8, 314–322.
- Huang, J., Chen, C., Axel, L., 2012. Fast multi-contrast MRI reconstruction, in: *Medical Image Computing and Computer-Assisted Intervention—MICCAI 2012. Springer*, pp. 281–288.

- Jones, R., Haraldseth, O., Müller, T., Rinck, P., Øksendal, A., 1993. K-space substitution: A novel dynamic imaging technique. *Magnetic resonance in medicine* 29, 830–834.
- Jung, H., Sung, K., Nayak, K.S., Kim, E.Y., Ye, J.C., 2009. k-t focuss: A general compressed sensing framework for high resolution dynamic MRI. *Magnetic Resonance in Medicine* 61, 103–116.
- Khajehnejad, M.A., Xu, W., Avestimehr, A.S., Hassibi, B., 2009. Weighted ℓ_1 minimization for sparse recovery with prior information, in: *Information Theory, 2009. ISIT 2009. IEEE International Symposium on*, IEEE. pp. 483–487.
- Knoll, F., Clason, C., Diwoky, C., Stollberger, R., 2011. Adapted random sampling patterns for accelerated MRI. *Magnetic Resonance Materials in Physics, Biology and Medicine* 24, 43–50.
- Korosec, F.R., Frayne, R., Grist, T.M., Mistretta, C.A., 1996. Time-resolved contrast-enhanced 3D MR angiography. *Magnetic Resonance in Medicine* 36, 345–351.
- Lang, T., Ji, J., 2008. Accelerating dynamic contrast-enhanced MRI using compressed sensing, in: *Proceedings of the 16th annual meeting of ISMRM*, Toronto, Canada, p. 1481.
- Lauzier, P.T., Tang, J., Chen, G., 2012. Prior image constrained compressed sensing: Implementation and performance evaluation. *Medical physics* 39, 66–80.
- Liang, D., DiBella, E.V., Chen, R., Ying, L., 2012. k-t ISD: Dynamic cardiac MR imaging using compressed sensing with iterative support detection. *Magnetic Resonance in Medicine* 68, 41–53.
- Liang, Z., Lauterbur, P., 1994. An efficient method for dynamic magnetic resonance imaging. *Medical Imaging, IEEE Transactions on* 13, 677–686.
- Lingala, S.G., Nadar, M., Ched'Hotel, C., Zhang, L., Jacob, M., 2011. Unified reconstruction and motion estimation in cardiac perfusion MRI, in: *Biomedical Imaging: From Nano to Macro, 2011 IEEE International Symposium on*, IEEE. pp. 65–68.

- Lustig, M., Donoho, D., Pauly, J.M., 2007. Sparse MRI: The application of compressed sensing for rapid MR imaging. *Magnetic resonance in medicine* 58, 1182–1195.
- Lustig, M., Santos, J.M., Donoho, D.L., Pauly, J.M., 2006. kt sparse: High frame rate dynamic MRI exploiting spatio-temporal sparsity, in: *Proceedings of the 13th Annual Meeting of ISMRM, Seattle*.
- Madore, B., Glover, G.H., Pelc, N.J., 1999. Unaliasing by fourier-encoding the overlaps using the temporal dimension (UNFOLD), applied to cardiac imaging and fMRI. *Magnetic Resonance in Medicine* 42, 813–828.
- McMillan, K., Uike, M., Tao, X., Kosugi, S., Okuda, H., 2010. MR efficiency becomes critical as healthcare costs, scanner time demand increases. *Signal Pulse of MRI Autumn 2010*, S10–S13.
- Mistretta, C., Wieben, O., Velikina, J., Block, W., Perry, J., Wu, Y., Johnson, K., 2006. Highly constrained backprojection for time-resolved MRI. *Magnetic resonance in medicine* 55, 30–40.
- Nagle, S.K., Levin, D., 1999. Multiple region MRI. *Magnetic resonance in medicine* 41, 774–786.
- Panych, L.P., Jolesz, F.A., 1994. A dynamically adaptive imaging algorithm for wavelet-encoded MRI. *Magnetic resonance in medicine* 32, 738–748.
- Ravishankar, S., Bresler, Y., 2011a. Adaptive sampling design for compressed sensing MRI, in: *Engineering in Medicine and Biology Society, EMBC, 2011 Annual International Conference of the IEEE, IEEE*. pp. 3751–3755.
- Ravishankar, S., Bresler, Y., 2011b. MR image reconstruction from highly undersampled k-space data by dictionary learning. *Medical Imaging, IEEE Transactions on* 30, 1028–1041.
- Rees, J., Watt, H., Jäger, H.R., Benton, C., Tozer, D., Tofts, P., Waldman, A., 2009. Volumes and growth rates of untreated adult low-grade gliomas indicate risk of early malignant transformation. *European journal of radiology* 72, 54–64.
- Samsonov, A.A., Velikina, J.V., Fleming, J.O., Schiebler, M.L., Field, A.S., 2010. Accelerated serial MR imaging in multiple sclerosis using baseline

- scan information, in: Proceedings of the 18th annual meeting of ISMRM, Stockholm, Sweden, p. 4876.
- Seeger, M., Nickisch, H., Pohmann, R., Schölkopf, B., 2010. Optimization of k-space trajectories for compressed sensing by bayesian experimental design. *Magnetic resonance in medicine* 63, 116–126.
- Tan, Z., Eldar, Y.C., Beck, A., Nehorai, A., 2014. Smoothing and decomposition for analysis sparse recovery. *Signal Processing, IEEE Transactions on* 62, 1762–1774.
- Trzasko, J.D., Haider, C.R., Borisch, E.A., Campeau, N.G., Glockner, J.F., Riederer, S.J., Manduca, A., 2011. Sparse-capr: Highly accelerated 4d CE-MRA with parallel imaging and nonconvex compressive sensing. *Magnetic Resonance in Medicine* 66, 1019–1032.
- Tsai, C., Nishimura, D.G., 2000. Reduced aliasing artifacts using variable-density k-space sampling trajectories. *Magnetic resonance in medicine* 43, 452–458.
- Tsaig, Y., Donoho, D., 2006. Extensions of compressed sensing. *Signal processing* 86, 549–571.
- Tsao, J., Boesiger, P., Pruessmann, K.P., 2003. k-t BLAST and k-t sense: Dynamic MRI with high frame rate exploiting spatiotemporal correlations. *Magnetic Resonance in Medicine* 50, 1031–1042.
- Van Den Berg, E., Friedlander, M.P., 2008. Probing the pareto frontier for basis pursuit solutions. *SIAM Journal on Scientific Computing* 31, 890–912.
- Van Vaals, J.J., Brummer, M.E., Thomas Dixon, W., Tuithof, H.H., Engels, H., Nelson, R.C., Gerety, B.M., Chezmar, J.L., Den Boer, J.A., 1993. keyhole method for accelerating imaging of contrast agent uptake. *Journal of Magnetic Resonance Imaging* 3, 671–675.
- Vaswani, N., Lu, W., 2010. Modified-cs: Modifying compressive sensing for problems with partially known support. *Signal Processing, IEEE Transactions on* 58, 4595–4607.

- Wei, D., Hero, A., 2013. Multistage adaptive estimation of sparse signals. *Selected Topics in Signal Processing*, IEEE Journal of 7, 783–796.
- Weizman, L., Ben Sira, L., Joskowicz, L., Constantini, S., Precel, R., Shofty, B., Ben Bashat, D., 2012. Automatic segmentation, internal classification, and follow-up of optic pathway gliomas in MRI. *Medical image analysis* 16, 177–188.
- Weizman, L., Ben Sira, L., Joskowicz, L., Rubin, D.L., Yeom, K.W., Constantini, S., Shofty, B., Ben Bashat, D., 2014. Semiautomatic segmentation and follow-up of multicomponent low-grade tumors in longitudinal brain MRI studies. *Medical physics* 41, 052303.
- Wu, H., Block, W.F., Samsonov, A.A., 2008. Hypr-constrained compressed sensing reconstruction for accelerated time resolved imaging, in: *Proceedings of the 16th annual meeting of ISMRM*, Toronto, Canada, p. 339.
- Yip, E., Yun, J., Wachowicz, K., Heikal, A.A., Gabos, Z., Rathee, S., Fallone, B., 2014. Prior data assisted compressed sensing: A novel MR imaging strategy for real time tracking of lung tumors. *Medical physics* 41, 082301.
- Yoo, S., Guttman, C., Zhao, L., Panych, L., 1999. Real-time adaptive functional MRI. *Neuroimage* 10, 596–606.
- Young, G.S., Macklin, E.A., Setayesh, K., Lawson, J.D., Wen, P.Y., Norden, A.D., Drappatz, J., Kesari, S., 2011. Longitudinal MRI evidence for decreased survival among periventricular glioblastoma. *Journal of neuro-oncology* 104, 261–269.
- Zientara, G.P., Panych, L.P., Jolesz, F.A., 1994. Dynamically adaptive MRI with encoding by singular value decomposition. *Magnetic Resonance in Medicine* 32, 268–274.
- Zonoobi, D., Kassim, A., 2012. Weighted-cs for reconstruction of highly under-sampled dynamic MRI sequences, in: *Signal Information Processing Association Annual Summit and Conference (APSIPA ASC)*, 2012 Asia-Pacific, IEEE. pp. 1–5.
- Zonoobi, D., Kassim, A.A., 2013. On the reconstruction of sequences of sparse signals—the weighted-cs. *Journal of Visual Communication and Image Representation* 24, 196–202.